5th Australasian Congress on Applied Mechanics, ACAM 2007
10-12 December 2007, Brisbane, Australia

# Variant Reorientation in Single-crystal Shape-memory Alloys

**H. Pan, *P. Thamburaja and* F.S. Chau**

*Department of Mechanical Engineering, National University of Singapore, Singapore*

*Abstract:* In this work we model the variant reorientation in a single crystal NiMnGa magnetic shape-memory alloy using the crystal-mechanics-based constitutive model of Thamburaja[1]. The model has been implemented in the ABAQUS/Explicit finite-element program by writing a user-material subroutine. Its numerical simulations quantitatively predict the mechanical response in simple compression and plain strain compression experiments to good accord.

*Keywords:* Crystal-mechanics, Finite-elements, Shape-memory alloy, Variant reorientation.

## 1 Introduction

Materials which are capable of undergoing reversible phase transitions e.g. shape-memory alloys, piezoelectric materials and ferromagnetic shape-memory alloys etc. are finding increased use as actuation devices in smart structures. These phase transitions typically occur between the high temperature phase, *austenite* and the low temperature phase, *martensite*. The cooling of these materials from its high temperature austenitic phase to below its *martensite finish temperature*, $\theta_{mf}$ will cause the conversion from the austenitic phase to multiple martensitic variants which are separated by twin planes or interfaces. The motion of these twin interfaces under the application of stress, electrical and magnetic fields will result in the conversion between martensitic variants i.e. *variant reorientation* and hence macroscopically observed shape changes.

The microscopic process of variant reorientation under stress can be schematically shown in Figure 1. As an example we consider the two variant case; variant i and variant j separated by a twin interface. Starting with the microstructure shown in state a, the application of stress from an unstressed state will cause the elastic deformation of the microstructures. Once a critical stress level is reached variant reorientation from variant *i* to variant *j* (state a $\rightarrow$ state b) will occur due to the motion of the twin interface. At state b, the variant reorientation would have been completed and further stressing will cause elastic deformation of the crystal. Conversely, applying the same level of stress in the opposite direction will cause variant reorientation from variant *j* to variant *i* (state a $\rightarrow$ state c) due to the motion of the twin interface. At state c, the variant reorientation would have been completed and further stressing will cause elastic deformation of the crystal.

## 2 Single-crystal constitutive model

For our constitutive model, we choose a representative-volume element (RVE) which contain martensitic variant(s) that originally nucleated from within a single crystal austenite i.e. state a in Figure 1, which is also taken as the reference configuration.

The governing variables in the constitutive model are: (i) The Helmholtz free energy per unit reference volume, $\psi$. (ii) The Cauchy stress, $T$. (iii) The deformation gradient, $F$ with $\det F > 0$. (iv) The inelastic deformation gradient, $F^p$ with $\det F^p > 0$. It represents the cumulative effect of martensitic variant reorientation in the RVE. (v) The elastic deformation gradient, $F^e = FF^{p-1}$ with $\det F^e > 0$. It describes the elastic distortion of the lattice that gives rise to the Cauchy stress $T$. (vi) The variant reorientation systems labelled by integers $ij$ with $i < j$ (to avoid the double counting of variant reorientation systems). Each potential variant reorientation system is then specified by a constant variant reorientation transition tensor, $S_0^{ij}$ which is assumed to be known in the reference configuration. (vii) The variant volume fractions in the RVE, $\xi^i$ with $0 \le \xi^i \le 1$ and $\chi = \sum_i \xi^i = 1$ representing the total martensite volume fraction.

The stress power per unit volume in the reference configuration is

$$\dot{w} = (\det F)T \cdot (\dot{F}F^{-1}).$$

This stress power may be additively decomposed as $\dot{w} = \dot{w}^e + \dot{w}^p$, where

$$\dot{w} = T^* \cdot \dot{E}^e$$

is the elastic stress power, with

$$E^e = \frac{1}{2}(F^{eT} F^e - 1) \text{ and } T^* = (\det F) F^{e-1} T F^{e-T}$$

denoting the Green elastic strain and the symmetric second Piola-Kirchoff stress tensor relative to the *reference* configuration, respectively. With $C^e = F^{eT} F^e$, the quantity

$$\dot{w}^p = (C^e T^*) \cdot (\dot{F}^p F^{p-1}) \geq 0 \tag{1}$$

is the inelastic stress power which is assumed to be strictly non-negative at all times.

**Free energy**

The Helmholtz free energy per unit *reference* volume (under isothermal conditions and in the fully-martensitic state) is taken to be

$$\psi = \frac{1}{2} E^e \cdot C[E^e] \text{ + constants} \tag{2}$$

where $C$ represents the constant fourth-order elasticity tensor.

**Constitutive equation for elastic stress**

The stress-strain constitutive equation is given by

$$T^* = \frac{\partial \psi}{\partial E^e} = C[E^e] \tag{3}$$

**Flow rule**

The evolution equation for the inelastic deformation gradient, $F^P$ is given by the flow rule:

$$\dot{F}^P = \left\{ \sum_{ij} \dot{\gamma}^{ij} S_0^{ij} \right\} F^p \tag{4}$$

where $\dot{\gamma}^{ij}$ denotes the *variant reorientation* rate between variant $i$ and variant $j$. Forward variant reorientation occurs when $\dot{\gamma}^{ij} > 0$, and reverse variant reorientation occurs when $\dot{\gamma}^{ij} < 0$.

Since the total martensite volume fraction is conserved during variant reorientation,

$$\dot{\xi}^i = \sum_{kl} H^{ikl} \dot{\gamma}^{kl}, \; k < l \tag{5}$$

with $i = 1, \ldots, P;\; k = 1, \ldots, P-1;\; l = 2, \ldots, P$. Here $P$ is the total number of variant reorientation systems and the interaction matrix is given by

$$H^{ikl} = \begin{cases} = 1 & if \quad i = k \\ = -1 & if \quad i > k \quad and \quad i = l \\ = 0 & if \quad otherwise \end{cases}$$

**Variant reorientation criteria**

Substituting equation (4) into inequality (1) yields

$$\sum_{ij} \sigma^{ij} \dot{\gamma}^{ij} \geq 0 \text{ with } \sigma^{ij} = (C^e T^*) \cdot S_0^{ij} \tag{6}$$

Here $\tau^{ij}$ represents the *driving force* on each variant reorientation system $ij$. Assuming the material to be *strongly dissipative*, inequality (6) will not be violated if we assume the condition

$$\tau^{ij}\dot{\gamma}^{ij} > 0 \quad \Rightarrow \quad sign(\tau^{ij}) = sign(\dot{\gamma}^{ij}) \quad if \quad \dot{\gamma}^{ij} \neq 0 \tag{7}$$

is satisfied for each variant reorientation system $ij$. Therefore with $\tau_c^{ij} > 0$ representing the constant *resistance* to variant reorientation, the variant reorientation criteria are

$$\Phi_+^{ij} \equiv \tau^{ij} - \tau_c^{ij} = 0 \text{ and } \Phi_-^{ij} \equiv \tau^{ij} + \tau_c^{ij} = 0 \tag{8}$$

for forward variant reorientation ($\dot{\gamma}^{ij} > 0$) and reverse variant reorientation ($\dot{\gamma}^{ij} < 0$), respectively. Finally the variant reorientation functions $\Phi_+^{ij}$ and $\Phi_-^{ij}$ are restricted as follows:

$$\Phi_+^{ij} \leq 0 \text{ and } \Phi_-^{ij} \geq 0$$

**Consistency conditions**

The consistency conditions that serve to determine the variant reorientation rates $\dot{\gamma}^{ij}$ are given as follows:

(1) If $\Phi_+^{ij} = 0, 0 \leq l^i < 1$ and $0 < l^j \leq 1$ then

$\dot{\gamma}^{ij}\dot{\Phi}_+^{ij} = 0$ for forward variant reorientation

(2) If $\Phi_-^{ij} = 0, 0 < l^i \leq 1$ and $0 \leq l^j < 1$ then

$\dot{\gamma}^{ij}\dot{\Phi}_-^{ij} = 0$ for reverse variant reorientation

For other conditions involving $\left\{\Phi_+^{ij}, \Phi_-^{ij}, l^i, l^j\right\}$, $\dot{\gamma}^{ij} = 0$.

Therefore the list of material parameters that needed to be calibrated are:

$$\left\{C, \tau_c^{ij}\right\}$$

The constitutive equations and a time-integration procedure have been implemented in the ABAQUS/Explicit (ABAQUS, [2]) by writing a user-material subroutine.

## 3 Determination of material parameters and FEM simulations

Originally austenitic single crystals of NiMnGa shape-memory alloys were purchased from a commercial source. At room temperature (298 K), these originally cubic austenitic single crystals have been transformed completely to the tetragonal martensitic phase, as shown in Figure 2. Following the methodology of Karaca et al. [3], these shape-memory alloys were compressed along the [100], [010] or [001]-direction of the parental cubic basis to make sure the material is initially in a single crystal martensitic variant state before subsequent testing takes place. Sufficient pure compression along the [100], [010] or [001]-direction of the parental cubic basis will result in the shape-memory alloy being in a fully single crystal martensite Variant 1, Variant 2 or Variant 3 state, respectively. Henceforth, we shall denote the [100], [010] and [001]-direction of the parental cubic basis as direction-1, direction-2 and direction-3, respectively.

Since there are no literature data on NiMnGa single crystals regarding its elastic moduli in the tetragonal phase, as a first-cut assumption, we will assume the elastic moduli $C$ to be isotropic. Hence, the rest of the material parameters needed to be calibrated from physical experiments are the Young's Modulus, E, the Poisson's ratio, $\nu$, the resistance to variant reorientation on each variant reorientation system, $\tau_c^{ij}$. In addition, we will assume that the resistance on all the variant reorientation systems are equal i.e. $\tau_c^{ij} = \tau_c$, and take the Poisson's ratio to be $\nu$ = 0:33 which is typical for a metallic alloy.

All the physical experiments performed in this work were conducted under very low strain/displacement rates to ensure that isothermal conditions prevail in the test specimens throughout the testing period. The experimental simple compression stress-strain data shown in Figure 3 was used to fit the material parameters E and $s_c^{ij}$ in our constitutive model. With the material initially being fully consisted of martensite Variant 3, a simple compression simulation along direction-2 was conducted to fit the material parameters in the constitutive model. This numerical simulation was conducted using a single ABAQUS C3D8R continuum-three dimensional brick element [3]. The values of the material parameters which best fit the experimental simple compression stress-strain curve shown in Figure 3 are:

- Elastic constants: Young's modulus, E = 2.5GPa; Poisson's ratio, $u$ = 0.33.
- Variant reorientation resistance: $s_c$ = 0.1606MJ/m$^3$.

The quality of the fit from this numerical simulation is shown in Figure 3. The constitutive model reproduces the experimental stress-strain curve to good accord. In particular, the constitutive model accurately predicts the amount of transformation strain ($\approx$6%) achieved in the physical experiment.

We then proceed to perform plane-strain compression simulations along direction-2 with the material being constrained along direction-1 or direction-3. The specimens for the plane-strain compression experiments have a cuboid geometry with their edges parallel along direction-1, direction-2 and direction-3. These test specimens have an initial height of 5.885mm measured along the loading direction (direction-2), and an initial width of 6.2mm measured along the constraint direction (direction-1 or direction-3). There is a small clearance of 0.02mm between the specimen and the constraints (which is assumed to be rigid) to allow for the insertion of the specimen into the actual testing setup.

The initially-undeformed mesh for the finite-element simulations which reproduce the actual experimental plane-strain compression conditions as explained above is shown in Figure 4. The test specimen is meshed using a single ABAQUS C3D8R element whereas the constraints along the sides of the specimen are meshed using two ABAQUS R3D4 rigid elements. A plane-strain compression simulation was conducted along direction-2 with the rigid constraints being applied along direction-1. Figure 3 shows the stress-strain response from this simulation plotted along with the stress-strain curve obtained from the corresponding physical experiment. The experimental stress-strain response is well-predicted by the constitutive model. Note that this simulation also accurately predicts the amount of transformation strain ($\approx$ 6%) observed in the physical experiment. The stress-strain response from this simulation is similar to the simulated stress-strain response in simple compression. The reason for this is as follows: Recall again that there is an initial separation of 0.02mm between the specimen and the rigid constraints as shown in Figure 4. Referring to the simulated stress-strain response shown in Figure 3, the critical stress for variant reorientation is reached at an applied strain of about 0.1 %. Even with the Poisson's effect at this magnitude of applied elastic deformation, the lateral sides of the specimen have still not come into contact with the rigid constraints. Further deformation will cause variant reorientation to occur along a constant stress plateau until the variant reorientation process is complete. During variant reorientation, the specimen will expand along direction-3 (the free direction) and no deformation will be experienced along direction-1 i.e. the specimen will still not come into contact with the rigid constraints. Thus no constraining stresses will be imposed on the specimen along direction-1 and direction-3, and the simulated stress-strain response plotted in Figure 3 will be similar to the simple compression stress-strain simulation result shown in Figure 3.

Next, using the initially-undeformed finite-element mesh shown in Figure 4, a plane-strain compression simulation was performed along direction-2 with the rigid constraints being applied along direction-3. The stress-strain curve from this simulation is plotted in Figure 3 along with the corresponding experimental stress-strain curve. The experimental stress-strain data is well-predicted by the constitutive model. However for the experimental and simulated stress-strain data shown in Figure 3, the variant reorientation process occurs along a stress plateau of about 0.34 % as compared to a stress plateau of 6 % obtained from the experimental and simulated stress-strain responses.

The reason for this observed difference can be explained as follows: Referring to the simulated stress-strain curve shown in Figure 3, the critical stress for variant reorientation is also reached at an applied strain of about 0.1 %. At an applied strain of about 0.1 %, the lateral sides of the specimen will

still not come into contact with the rigid constraints even with the Poisson's effect accompanying the applied elastic deformation thus far. A further application of deformation will result in the variant reorientation process to occur along a constant stress plateau. During the conversion from Variant 3 to Variant 2, the specimen will expand along direction-3 (the constraint direction) with no further deformation occurring along direction-1 (the free direction). At an applied strain of approximately 0.44 %, the specimen would have expanded enough along direction-3 to be in contact with the rigid constraints. Upon further deformation, the variant reorientation process will continue with a steep increase in the magnitude of the loading stress i.e. the variant reorientation process will not occur at a constant loading stress level anymore. This is because of the increasing magnitude of the constraint stresses with increasing applied deformation.

## 3 Conclusions

In conclusion, the constitutive model is able to *quantitatively* and *qualitatively* capture the exotic stress-strain behavior exhibited by these shape-memory alloys, under simple compression and plane-strain compression loading conditions.

## References


[1]. Thamburaja P (2005) Constitutive equations for martensitic reorientation and detwinning in shape-memory alloys. J Mech Phys Solids, 53: 825-856

[2]. ABAQUS Reference Manuals (2006) Providence, R.I.

[3]. Karaca, H., Karaman, I., Basaran, B., Chumlyakov, Y., & Maier, H. (2006). Magnetic field and stress induced martensite reorientation in NiNnGa ferromagnetic shape memory alloy single crystals. Acta Materialia, 54: 233-245.


## Figures

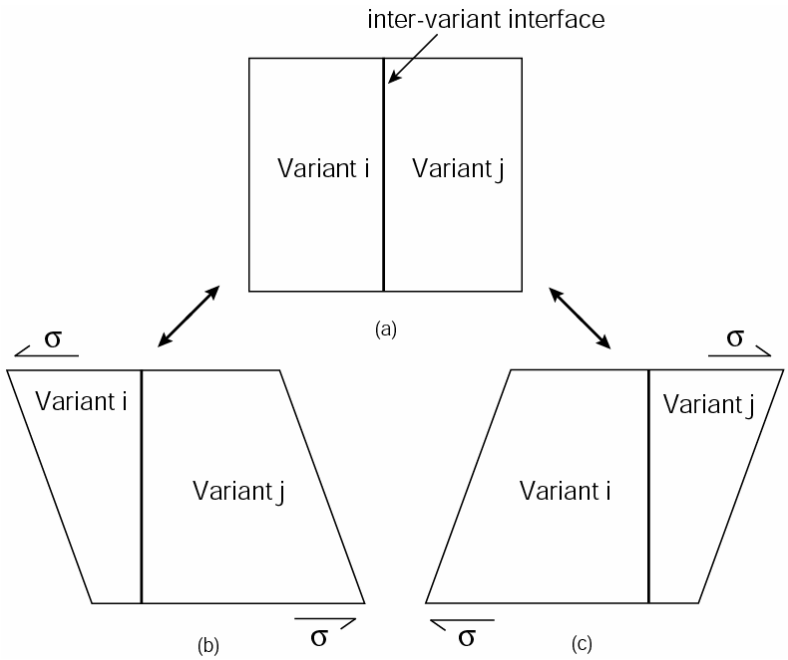


Figure 1: Martensitic variants i and j originated from a single crystal austenite separated by an inter-variant/twin interface. Under stress $S$, the microstructure shown in (a) will undergo variant reorientation and transform into the microstructures shown in (b) or (c) depending on the sign of stress. Transformation between the microstructures shown in (b) and (c) is assumed to go through stage (a).

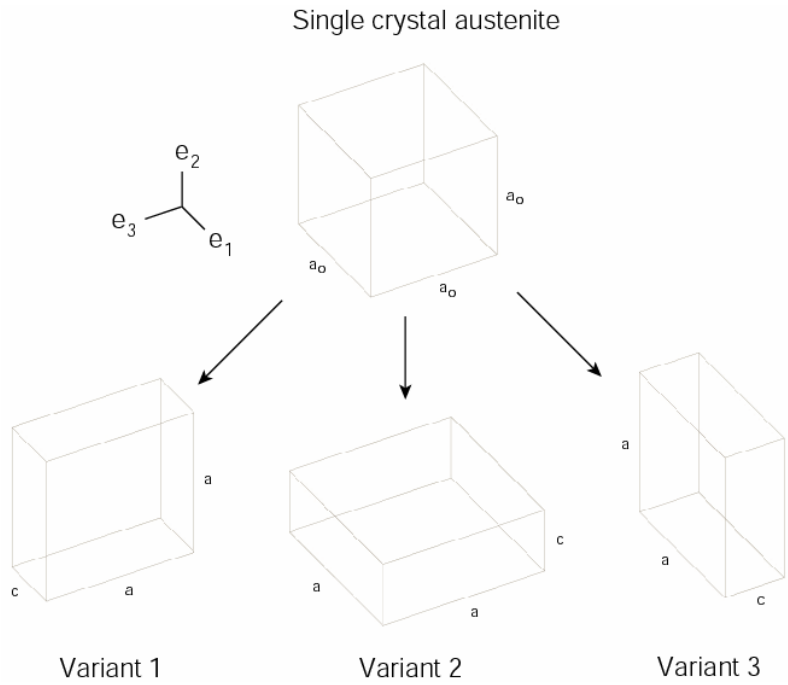


Figure 2: Austenite to martensite transformation of a single crystal NiMnGa shape-memory alloy. The cubic parent austenitic phase can transform into three tetragonal martensitic variants i.e. the [100] (Variant 1), [010] (Variant 2) and [001] (Variant 3) variants. The lattice parameters for both the crystal structures are also shown.

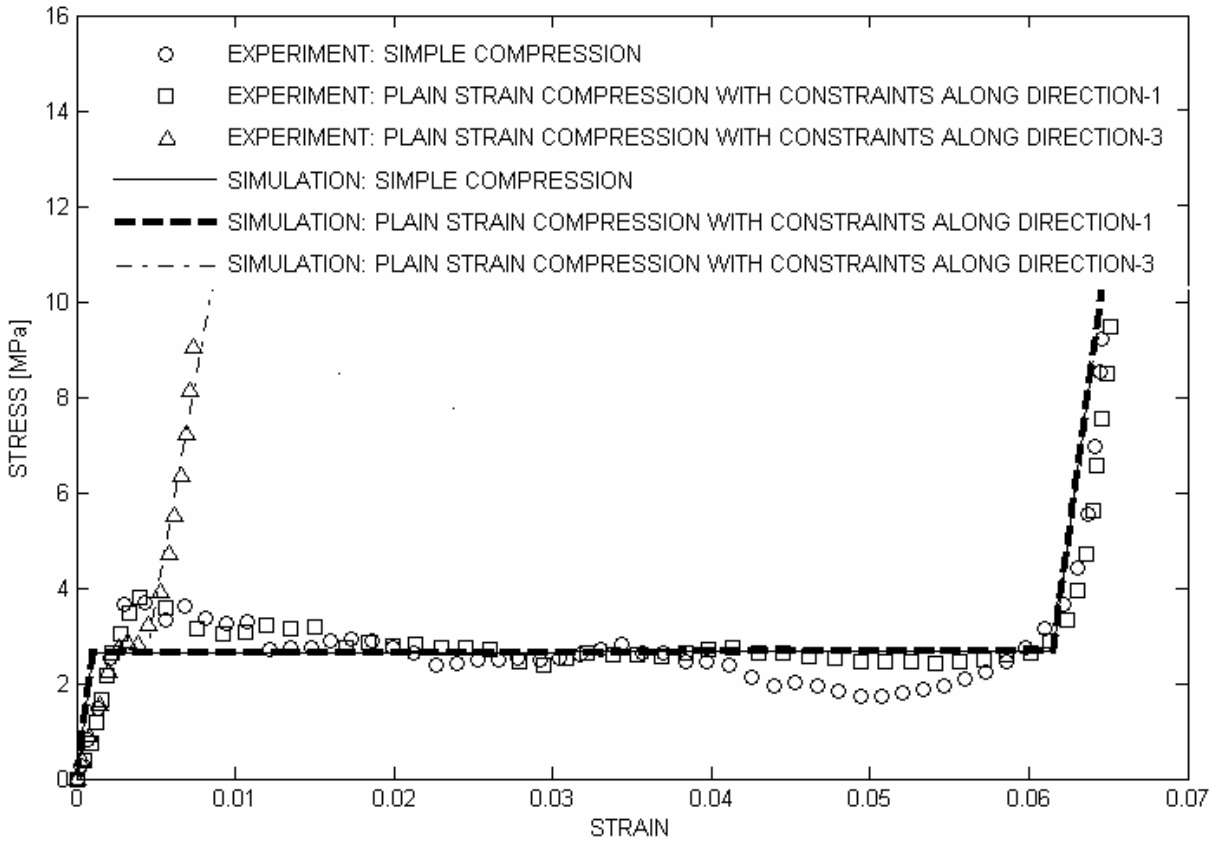


Figure 3: Experimental stress-strain curve in a simple compression experiment, plain-strain compression experiment with constraints along direction-1 and plain-strain compression experiment with constraints along direction-3. The numerical predictions from the corresponding finite-element simulation are also shown.

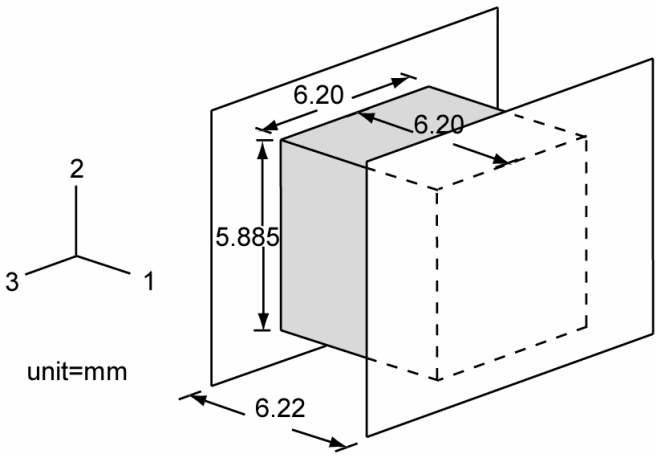


Figure 4: The initially-undeformed mesh for the finite-element simulations which reproduce the actual experimental plane-strain compression conditions. All dimensions are in milimeter.